

# Degradation-Adaptive Neural Network for Jointly Single Image Dehazing and Desnowing

Erkang Chen<sup>†</sup>, Sixiang Chen<sup>†</sup>, Tian Ye, Yun Liu

**Abstract**—Removing adverse weather conditions such as haze and snow from a single image is a challenging problem. Although existing image restoration algorithms focusing on one type of specific degradation have made impressive progresses, they are not flexible enough to deal with multiple degradation types. Therefore, we propose a lightweight image restoration network called Degradation-Adaptive Neural Network (DAN-Net) to achieve jointly single image dehazing and desnowing, which consists of two compact expert networks and an adaptive gated neural. The expert networks relying on three novel components is proposed to address specific haze or snow degradation in nasty winter scenes. Based on the Mixture-of-Experts (MoE) strategy, the proposed DAN-Net captures degradations from each input image to adaptively modulate the outputs of task-specific expert networks for removing various adverse winter weather conditions. Specifically, DAN-Net adopts a novel adaptive gated neural network to predict gated attention maps of the input image, while different task-specific experts with the same topology are jointly dispatched to deal with the degraded image. In this way, the proposed approach can effectively handle different types of severe weather scenarios. Experiments verify that our proposed method performs over state-of-the-art dehazing and desnowing techniques on synthetic datasets and real-world images.

**Index Terms**—Single image dehazing and desnowing, degradation-adaptive neural network (DAN-Net), mixture-of-experts (MoE), expert network, adaptive gated neural

## I. INTRODUCTION

In nasty winter scenes, the acquired images will be adversely degraded by haze and snow. Therefore, many high-level computer vision tasks that requires high-quality inputs, such as object recognition, tracking and person reidentification, urgently need trustworthy image restoration algorithms. Recently, several end-to-end learning-based methods [5]–[11], [18], [20]–[24], [27], [28], [30] have been proposed to achieve image recovery by directly learning the mapping from a degraded image to a clear image, which have made remarkable successes in the community of image restoration. However, owing to the complexity of multiple degrading effects, most existing image restoration methods only perform well on one type of degradation by lousy weather (e.g. hazy and snowy) and are incapable of handling multiple types of degradations. In real-world snow scenarios, the captured degraded image usually contains diverse snow streaks and

snowflakes and also suffers from the uneven haze effect, resulting in a more challenging image restoration task.

In daily winter scenes, the uneven haze often occurs with diverse snowy degradation and the widely used haze imaging model [13] is modeled as:

$$\mathcal{I}(x) = \mathcal{J}(x)t(x) + \mathcal{A}(1 - t(x)) \quad (1)$$

where  $t(x)$  is the transmission map of hazy image  $\mathcal{I}(x)$ , and  $\mathcal{A}$  is the global atmospheric light. Single image dehazing methods aim to recover the clean image  $\mathcal{J}(x)$  from  $\mathcal{I}(x)$ . Owing to the ill-posed problem, some works employ the fusion-based [35], [37] or contrast correction [17] to promote the visual effects of the hazy image. However, the performance of these methods are limited.

Similarly, on the basis of the previous works [6], [7], the formation of snow is modeled as:

$$\mathcal{I}(x) = \mathcal{K}(x)\mathcal{T}(x) + \mathcal{A}(x)(1 - \mathcal{T}(x)) \quad (2)$$

where  $\mathcal{K}(x) = \mathcal{J}(x)(1 - \mathcal{Z}(x)\mathcal{R}(x)) + \mathcal{C}(x)\mathcal{Z}(x)\mathcal{R}(x)$ ,  $\mathcal{I}(x)$  represents the snowy image,  $\mathcal{K}(x)$  denotes the veiling-free snowy image,  $\mathcal{T}(x)$  is the media transmission map,  $\mathcal{A}(x)$  is the atmospheric light and  $\mathcal{J}(x)$  is the snow-free image.  $\mathcal{C}(x)$  and  $\mathcal{Z}(x)$  are the chromatic aberration map for snow images and the snow mask, respectively.  $\mathcal{R}(x)$  is the binary mask, presenting the snow location information.

Obviously, the incompatibility of physical models implies a considerable challenge to remove haze and snow for a single compact network coordinately. The diverse degradation scale of the snow and the uneven density of natural haze lead to a high threshold for efficient implementation.

Based on the aforementioned analysis, most existing methods have been designed to overcome only one type of degradation. Recently, a CNN-based universal method, *i.e.*, All-in-One [20], is proposed to remove all weather conditions at once. However, this method is limited in the real-world practical application due to the heavy amount of parameters, and it also ignores the implicit useful knowledge in different types of degradation to boost the performance of the model.

To achieve practical real-world winter image restoration, we propose a lightweight Degradation-Adaptive Neural Network (DAN-Net) based on the Mixture of Experts (MoE) strategy to jointly achieve dehazing and desnowing from a single degraded image. The proposed DAN-Net consists of three parts: two task-specific expert networks and an adaptive gated neural. Specifically, three novel high-performance components are carefully devised to construct the expert network: Multi-branch Spectral Transform Block (MSTB) based on Fast Fourier Convolution and multi-scale filter to address the diverse scale

<sup>†</sup>Equal contribution.

E. Chen, S. Chen and T. Ye are with School of Ocean Information Engineering, Jimei University, Xiamen, China (e-mail: ekchen@jmu.edu.cn, 201921114013@jmu.edu.cn, 201921114031@jmu.edu.cn )

Y. Liu is with College of Artificial Intelligence, Southwest University, Chongqing, China (e-mail: yunliu@swu.edu.cn).

Corresponding author: Yun Liu

degradation, Dual-Pool Attention Module (DPAB) to refine the uneven features of real-world degradation, and Cross-Layer Activation Gated Module (CLAGM) to optimize information flow of features with different scales. To our surprise, the designed lightweight dehazing and desnowing expert networks can achieve best performance-parameter trade-off in contrast to previous state-of-the-art single-task algorithms. In addition, to skillfully combine the expert network with different task knowledge, a novel adaptive gated neural is developed to learn the inner knowledge of expert networks for simultaneously removing haze and snow degradations. Experiments show that the proposed DAN-Net as an efficient and effective image restoration solution addresses diverse degradation in winter scenes, such as complex, uneven hazy effects, and snow particles, streaks, and patches. The main contributions are summarized as follows:

- Considering multiple degrading effects (haze and snow) under real-world winter scenes, a lightweight DAN-Net consisting of two compact task-specific expert networks and an adaptive gated neural is proposed to achieve jointly single image dehazing and desnowing.
- Three effective modules (MSTB, DPAB and CLAGM) as the fundamental components are designed to construct a task-specific expert network, which achieves best trade-off between restoration performance and parameters for image dehazing and desnowing.
- To fully make use of the performance of two task-specific expert networks, the presented adaptive gated neural is considered as an effective degradation-adaptive guider to control the contributions of two pre-trained expert networks, which contributes to removing multiple degradations.
- Extensive experiments demonstrate that the proposed DAN-Net can provide satisfactory results for both synthetic and real-world degraded images under winter scenes, which performs favorably against other state-of-the-art dehazing or desnowing algorithms in subjective and objective evaluations.

## II. RELATED WORK

In this section, we will briefly review some recent image restoration algorithms including single image dehazing and desnowing. To the best of our knowledge, the existing dehazing and desnowing approaches can be classified into two categories: prior-based methods and learning-based methods.

### A. Single Image Dehazing

**Prior-based Dehazing Methods.** Haze removal from a single image is a ill-posed image restoration problem because of too many unknown parameters. Therefore, researchers make use of various priors, such as dark channel prior (DCP) [13], color-lines prior [12], color attenuation prior [36], color ellipsoid prior [4], haze-lines prior [3], gamma correction prior [16] and region lines prior [15], to estimate the parameters of the physical model. The most well-known DCP exploit the dark channel to predict the transmission map whose principle is based on the statistical observation that the minimum pixel

intensity in the non-sky patches of the clear image is usually close to zero. Although prior-based dehazing methods perform haze removal well, they cannot reconcile the weaknesses of limiting by sophisticated scenes because these presented priors are not always suitable for complex real-world scenarios.

**Learning-based Dehazing Methods.** To overcome the prior dependency, numerous learning-based dehazing methods [5], [9], [10], [18], [21]–[23], [27], [28], [30] are gradually proposed to learn the mapping relationship between a hazy image and a haze-free image. DehazeNet [5] and MSCNN [28] are developed to achieve the end-to-end mapping from a hazy image to the transmission map of the physical model. FFA-Net [27] devise an attention network for feature map fusion by combining pixel attention and channel attention for image dehazing. Dong *et al.* [10] presented a multi-scale boosted dehazing network with dense feature fusion based on the U-Net backbone. For solving the domain gap problem between real and synthetic samples, Shao *et al.* [30] develop a domain adaptation framework consisting of a bidirectional translation module and two image dehazing modules to improve the generalization performance on real-world hazy images. Compared with the traditional dehazing methods, these learning-based dehazing methods are able to realize better dehazing performance. However, existing methods fail to handle other types of degradations apart from the haze.

### B. Single Image Desnowing

**Prior-based Desnowing Methods.** Early approaches [26], [31]–[34] exploit hand-crafted priors to achieve snow removal from a single snowy image. Pei *et al.* [26] make use of features on saturation and visibility to remove the snowflakes. In [32], a guidance image method is proposed to remove snow from a single image. Based on the difference between background edges and rain streaks, Zheng *et al.* [34] adopt multi-guided filter to extract the features for splitting the snowy component from the background. Wang *et al.* [31] develop a three layer hierarchical scheme for desnowing by leveraging image decomposition and dictionary learning. Unfortunately, these prior-based methods have several limitations for real-world scenes cannot remove the snow thoroughly due to complex degradations caused by different size and types of snow such as snowflakes and snow particles.

**Learning-based Desnowing Methods.** For learning-based desnowing algorithms [6]–[8], [11], [20], [24], the first presented desnowing network called DesnowNet [24] deals with the removal of translucent and opaque snow particles in sequence based on a multi-stage learning architecture. JS-TASR [6] propose a novel snow formation model and size-aware snow network for single image desnowing which takes the veiling effect and variety of snow particles into consideration. HDCW-Net [7] performs snow removal by embedding the dual-tree wavelet transform into the architecture of the network and designing prior-based supervised loss called the contradict channel on the basis of the differences of snow and clean images. Li *et al.* [20] develop an all-in-one network consisting of multiple task-specific encoders that can simultaneously handle multiple types of bad weather scenarios, such as rain, snow,

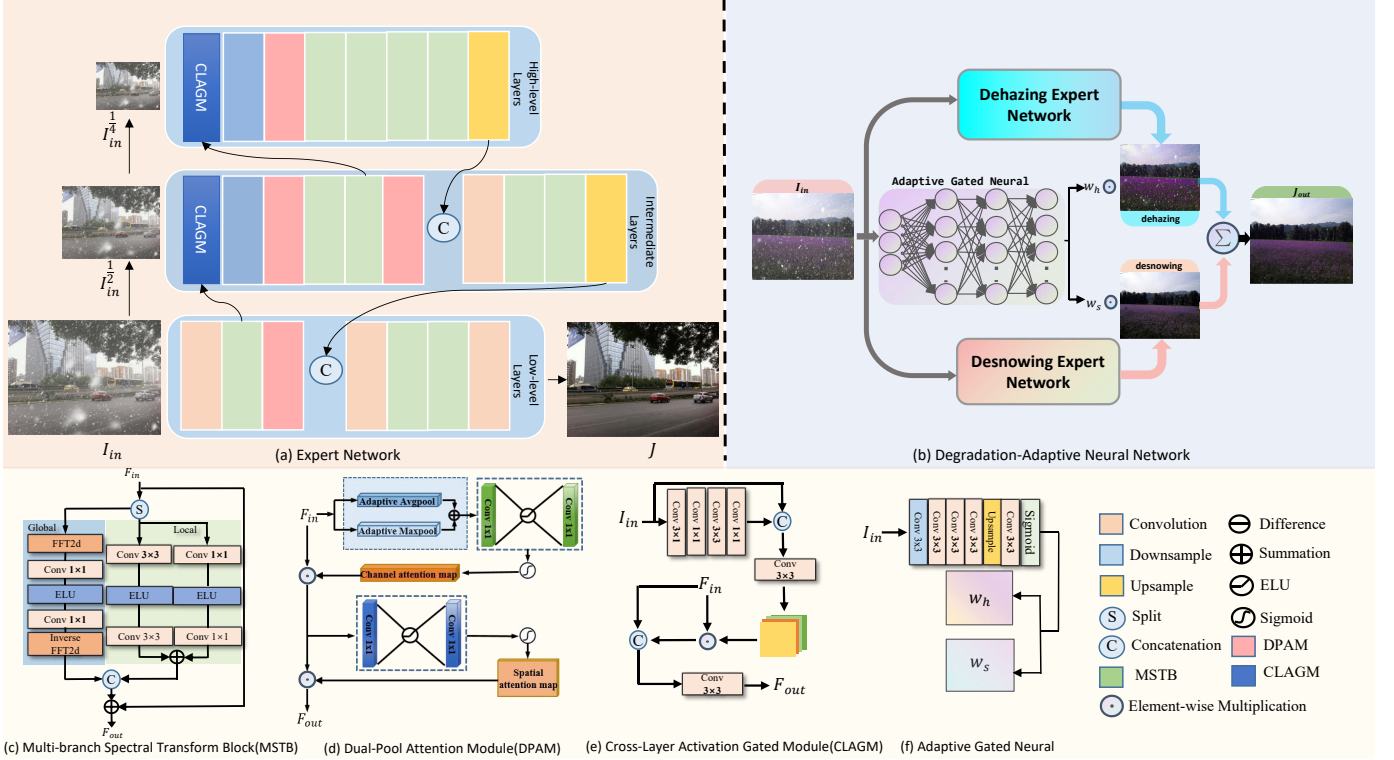


Fig. 1: The schematic illustration of the proposed degradation-adaptive neural network (DAN-Net). DAN-Net consists of three parts: (a) task-specific expert dehazing and desnowing networks and (f) adaptive gated neural module. The expert network includes three compact components: (c) MSTB, (d) DPAM and (e) CLAGM. The expert dehazing and desnowing networks are firstly well-trained and then the adaptive gated neural module is employed to dynamically control the activation of expert networks for coordinated removing haze and snow from a winter degraded image.

haze and raindrops. Meantime, two large-scale snow datasets dubbed as snow removal in realistic scenario (SRRS) and comprehensive snow dataset (CSD) are respectively proposed in [6] and [7] for promoting the development of learning-based image desnowing methods. These above methods are incapable to removing the uneven haze effects in the snowy image.

### III. TASK-SPECIFIC EXPERT NETWORK

In this section, we present the overall architecture of the proposed task-specific expert network, shown in Fig. 1(a). Concretely, three high-performance convolution-based components (i.e. MSTB, DPAM and CLAGM) and three-level layers are carefully designed to construct the lightweight expert network, as depicted in Fig. 1(c)-(e). Different from previous learning-based methods [6], [10], [23], [27] that simply stack the components repeatedly to achieve impressive performance, our presented expert network deliberately avoids this strategy and achieves excellent parameter-performance trade-off through careful design in each layer and as few components as possible. Next, we describe the details of three components and three-level layers.

**Dual-pool Attention Module (DPAM).** The effectiveness of the attention module for the feature representation ability of the network has been demonstrated in the image restoration task. To improve the performance of the expert network, we introduce the dual-pool attention module into our network. As observed in Fig. 1(d), we make use of the AvgPool and

Maxpool to sample the incoming features for the generation of channel dimension weights:

$$\begin{aligned} \text{AvgPool} : \mathbb{R}^{H \times W \times C} &\rightarrow \mathbb{R}_{avg}^{1 \times 1 \times C} \\ \text{MaxPool} : \mathbb{R}^{H \times W \times C} &\rightarrow \mathbb{R}_{max}^{1 \times 1 \times C} \end{aligned} \quad (3)$$

Then, we add the sampled features and adopt the convolution block to generate the attention weights of channel dimension:

$$\text{Conv} \circ \text{ELU} \circ \text{Conv with } 1 \times 1 : \mathbb{R}_{avg}^{1 \times 1 \times C} + \mathbb{R}_{max}^{1 \times 1 \times C} \rightarrow \mathbb{R}^{1 \times 1 \times C} \quad (4)$$

The *Sigmoid* function is used to keep the boundary of final attention weights:

$$\text{Sigmoid} : \mathbb{R}^{1 \times 1 \times C} \rightarrow \mathbb{R}_c^{1 \times 1 \times C}, \quad (5)$$

The attention mechanism in spatial dimension is also necessary for refining the features. The plain convolution block can generate the attention map in 2D dimension:

$$\text{Conv} \circ \text{ELU} \circ \text{Conv with } 1 \times 1 : \mathbb{R}^{H \times W \times C} \rightarrow \mathbb{R}^{H \times W \times \frac{C}{r}} \rightarrow \mathbb{R}^{H \times W \times 1}, \quad (6)$$

where \$r\$ is the scale-factor, we set it as 4 for all experiments. The *Sigmoid* function constrains the final spatial attention map:

$$\text{Sigmoid} : \mathbb{R}^{H \times W \times 1} \rightarrow \mathbb{R}_s^{H \times W \times 1}, \quad (7)$$

**Multi-branch Spectral Transform Block (MSTB).** Considering the uneven distribution of features in channel dimension in neural networks, we assume that the information from

a part of the channel in incoming features can help network to establish global dependencies by spectral transformation. Consequently, the designed MSTB splits the incoming features  $\mathbb{R}_{in}$  as:

$$\mathbb{R}_{in}^{H \times W \times C} \rightarrow \mathbb{R}_g^{H \times W \times \frac{C}{2}}, \mathbb{R}_l^{H \times W \times \frac{C}{2}} \quad (8)$$

Then, the global branch of MSTB performs Fast Fourier Convolution (**FFC**) on the  $\mathbb{R}_g^{H \times W \times \frac{C}{2}}$ . As shown in Fig. 1(c), the global branch adopts real FFT to account for global context. This designed parallel multi-branch combines different scale operation in single block, effectively capturing local information and global dependencies simultaneously and avoiding heavy computational burden for a lightweight network. Specifically, the global branch first applies 2D Real FFT to the input features:

$$\text{Real FFT 2d} : \mathbb{R}_g^{H \times W \times \frac{C}{2}} \rightarrow \mathbb{C}^{H \times \frac{W}{2} \times \frac{C}{2}} \quad (9)$$

and then concatenates real and imaginary part for the subsequent feature extraction:

$$\text{ComplexToReal} : \mathbb{C}^{H \times \frac{W}{2} \times \frac{C}{2}} \rightarrow \mathbb{R}^{H \times \frac{W}{2} \times C} \quad (10)$$

Afterwards, we applies the convolution block with the kernel size of  $1 \times 1$  in the frequency domain for capturing the long-distance dependence:

$$\text{Conv} \circ \text{ELU} \circ \text{Conv} : \mathbb{R}^{H \times \frac{W}{2} \times C} \rightarrow \mathbb{R}^{H \times \frac{W}{2} \times C} \quad (11)$$

Finally, the inverse transformation is employed to recover the spatial structure of features:

$$\begin{aligned} \text{RealToComplex} &: \mathbb{R}^{H \times \frac{W}{2} \times C} \rightarrow \mathbb{C}^{H \times \frac{W}{2} \times \frac{C}{2}} \\ \text{Inverse Real FFT2d} &: \mathbb{C}^{H \times \frac{W}{2} \times \frac{C}{2}} \rightarrow \mathbb{R}_{ff2d}^{H \times W \times \frac{C}{2}}, \end{aligned} \quad (12)$$

In addition, we exploit multi-scale convolution blocks as local branch to capture the local information, as more important as global information in the procedure of details restoration:

$$\begin{aligned} \text{Conv} \circ \text{ELU} \circ \text{Conv with } 1 \times 1 &: \mathbb{R}_l^{H \times W \times \frac{C}{2}} \rightarrow \mathbb{R}_3^{H \times W \times \frac{C}{2}} \\ \text{Conv} \circ \text{ELU} \circ \text{Conv with } 3 \times 3 &: \mathbb{R}_l^{H \times W \times \frac{C}{2}} \rightarrow \mathbb{R}_1^{H \times W \times \frac{C}{2}}, \end{aligned} \quad (13)$$

Finally, we fuse all features from each branch and perform local residual learning by concatenate and add operator:

$$\begin{aligned} \text{Fusion} &: \mathbb{R}_{ff2d}^{H \times W \times \frac{C}{2}} + \mathbb{R}_3^{H \times W \times \frac{C}{2}} \\ &\quad + \mathbb{R}_1^{H \times W \times \frac{C}{2}} + \mathbb{R}^{H \times W \times C} \rightarrow \mathbb{R}_{out}^{H \times W \times C} \end{aligned} \quad (14)$$

The proposed MSTB effectively captures the global context information and the local features, which achieves excellent trade-off in complexity and modeling-ability due to the channel splitting solution and fast Fourier convolution.

**Cross-Layer Activation Gated Module (CLAGM).** The information loss caused by repetitive down-sampling seems unavoidable in a multi-scale feature flow network. The recent research [29] reveals that the retinal ganglion cells and cerebral visual cortex cells have a whole new way of cell communication, which is mediated by exosomes different from synapses. Inspired by this idea, we find that the additional external information can bring the valuable activation like an instructor for the current layer. Thus we hope that external information

from the down-sampled original image to effectively regulate the input features from another layer. As observed in Fig. 1(e), a series of operations are preformed on  $I_{in}^{\frac{1}{2}}$  or  $I_{in}^{\frac{1}{4}}$  to generate the activation gated map  $\mathcal{M}^{H \times W \times C}$ :

$$\mathcal{M}^{H \times W \times C} = \text{CLAGM}(I_{in}^{H \times W \times 3}), \quad (15)$$

where the  $\mathcal{M}^{H \times W \times C}$  is a unique attention map from additional information, whose size is the same as the  $\mathbb{R}_{in}$ . Then, we multiply  $\mathcal{M}$  with input feature  $\mathbb{R}_{in}$ :

$$\mathbb{R}_{gated}^{H \times W \times C} = \mathcal{M}^{H \times W \times C} \cdot \mathbb{R}_{in}^{H \times W \times C}, \quad (16)$$

Afterwards, the original  $\mathbb{R}_{in}$  and the weighted  $\mathbb{R}'_{in}$  are fused by channel merging and compressing:

$$\text{Conv with } 3 \times 3 : \mathbb{R}_{in}^{H \times W \times C} + \mathbb{R}_{gated}^{H \times W \times C} \rightarrow \mathbb{R}_{out}^{H \times W \times C} \quad (17)$$

The proposed cross-scale mechanism can help the network better exploit the inner knowledge of the original degraded images and optimize the information flow over the network.

**Lower-level Layers:** First of all, the designed lower-level layers as the level one role to extract the features from original degenerated images in the original resolution. In Fig. 1(a), a  $3 \times 3$  convolution is used to extract the features with 32 channels (16 channels in the tiny version). Second, these features will be sent into the intermediate layers and the subsequent attention module. Then, the concatenate operation is exploited to fuse the features that feed back from the intermediate layers and the refined features by the attention module, thus aggregating the features with 64 channels (32 channels in the tiny version):

$$\text{Concatenate: } \mathbb{R}_S^{H \times W \times 32} + \mathbb{R}_I^{H \times W \times 32} \rightarrow \mathbb{R}_S^{H \times W \times 64}, \quad (18)$$

where the  $\mathbb{R}_I^{H \times W \times 32}$  is the features from the intermediate layers. In addition, we perform the  $3 \times 3$  convolution to compress the channel of features.

$$\text{Conv with } 3 \times 3 : \mathbb{R}_S^{H \times W \times 64} \rightarrow \mathbb{R}_S^{H \times W \times 32}, \quad (19)$$

From Fig. 1(a), two cascaded MSTB and a  $3 \times 3$  convolution are employed to provide the final clean image  $J$  from features.

**Intermediate Layers:** As depicted in Fig. 1(a), the structured intermediate layers as a transmitter and a receiver coordinates the complex information flow and enhances the coupling of each layer in the expert network. Specifically, the number of the channel of MSTB and DPAM only is 64 (32 in the tiny version) in this layer, and CLAGM receives the  $\frac{1}{2}$  down-sampled degenerated images to aggregate and refines features. In the proposed task-specific expert network, the intermediate layers play a vital role as a powerful connection between different layers, owing most complex features from different scales and refining them for exploring deep, valuable features.

**High-level Layers:** The designed high-level layers are responsible for extracting more information in high dimension space from features with 128 channels (64 channels in tiny version) and  $\frac{1}{4}$  size. In Fig. 1(a), with the help of  $\frac{1}{4}$  down-sampled degenerated images and external features from the intermediate layers, the high-level layers helps the designed expert network to generate more pleasant clean images from degraded winter images.

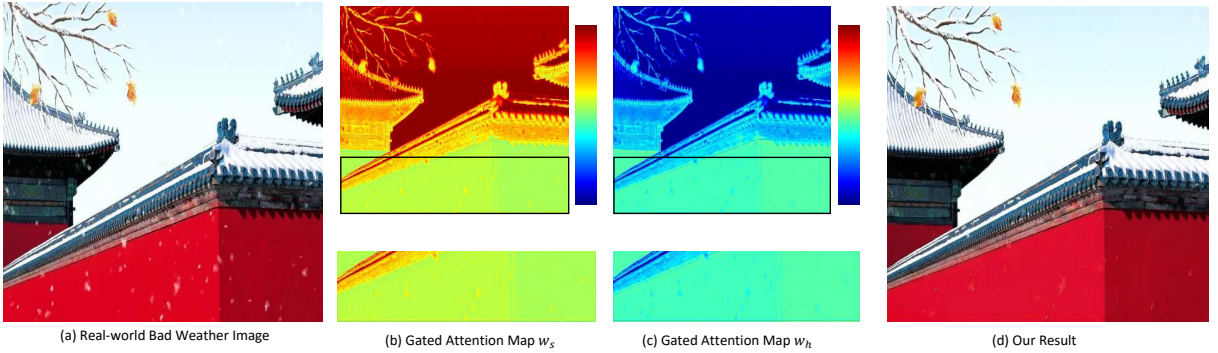


Fig. 2: Illustration of the gated attention maps. (a) and (d) are the real-world bad weather image and the corresponding restoration result. (b) and (c) are two gated attention maps  $w_s, w_h$  corresponding to the desnowing and dehazing expert activation intensity, respectively.

#### IV. DEGRADATION-ADAPTIVE NEURAL NETWORK

The MoE strategy [14], [25] is an effective long-standing solution that exploits the integration of multiple expert networks to improve single-task performance. A trainable gating network is usually employed to produce the gated weights for activating each expert network based on an explicit or implicit partition of the input data, for instance, labels, classes (explicit) or contextual content features (implicit). In the DAN-Net, the proposed adaptive gated neural learns how to generate the gated attention maps as the activating weight, according to the uncertain degradation of the input winter image without explicit signal. Besides, instead of the intent of improving single-task performance in previous methods [1], [25], the adaptive mechanism is adopted based on MoE and the rich inner knowledge of task-specific expert networks, which can not only address the uncertain multi-degradation problem but also boost the comprehensive performance of DAN-Net in winter nasty scenes. Such a novel image restoration pipeline is effective and efficient due to the degradation-adaptive mechanism and well-learned expert networks with lightweight architecture.

Specifically, a adaptive gated neural is devised as the guider to adaptively control the contribution of two different pre-trained expert networks. For real-world winter conditions, the captured degraded image usually suffers from the uneven spatial distribution and different types of degradations. In order to circumvent this issue, the 2D attention map is considered as the gated map to address these degraded attributes for better performance. In Fig. 1(b) and Fig. 1(f), the adaptive gated neural predicts the gated attention map  $w_s \in \mathbb{R}^{1 \times H \times W}, w_h \in \mathbb{R}^{1 \times H \times W}$  based on the input degraded images:

$$w_h, w_s = \text{AGN}(I_{in}), \quad (20)$$

where **AGN** denotes the adaptive gated neural, and  $w_h, w_s$  denote the gated attention map for dehazing and desnowing results, respectively. Then we multiply the gated attention map  $w_h$  and  $w_s$  with  $J_{dehazing}, J_{desnowing}$  generated by dehazing expert and desnowing expert networks, respectively:

$$J_{out} = w_h \cdot J_{dehazing} + w_s \cdot J_{desnowing} \quad (21)$$

where  $J_{out}^{3 \times H \times W}$  is the final result of the proposed DAN-Net.

Experiments demonstrate that the usage of the adaptive gated mechanism is beneficial for the performance of both

dehazing and desnowing tasks and our DAN-Net achieves better performance on both tasks than single task-specific expert network. Fig. 2 depicts the obtained gated attention maps from a real-world bad weather image and the corresponding restoration result. From Fig. 2(b) and Fig. 2(c), the snowy degradation regions in  $w_s$  have higher activation intensity than  $w_h$  and other areas, which indicates the effectiveness of the proposed adaptive gated neural module.

#### V. LOSS FUNCTION

The proposed DAN-Net is trained in an end-to-end manner using a Charbonnier loss as the basic reconstruction loss between the prediction and the ground truth, which is defined as follows:

$$\mathcal{L}_{char} = \frac{1}{N} \sum_{i=1}^N \sqrt{\|X^i - Y^i\|^2 + \epsilon^2}, \quad (22)$$

where  $\epsilon$  is empirically set as  $10^{-3}$  for all the experiments,  $X^i$  denotes the generated image of network and  $Y^i$  correspondingly denotes the ground truth. In addition, we also add the spectral transform to evaluate the difference of the reconstructed images and the ground truth images in the frequency domain:

$$\mathcal{L}_{st} = \|\mathcal{F}(\mathbf{J}_{clean}) - \mathcal{F}(\mathbf{J}_{gt})\|_1, \quad (23)$$

where  $\mathcal{F}$  denotes the FFT operation,  $\mathbf{J}_{clean}$  denotes the generated images of our network, and  $\mathbf{J}_{gt}$  denotes the ground truth images. The spectral transform loss function is remarkably beneficial to the improvement of SSIM. The overall loss function are summarized as follows:

$$\mathcal{L}_{expert} = \mathcal{L}_{char} + \lambda_{st} \mathcal{L}_{st} \quad (24)$$

where  $\lambda_{st}$  is the trade-off weight.

#### VI. EXPERIMENTS

##### A. Datasets and Metrics

We choose the widely used PSNR and SSIM as experimental metrics to measure the performance of our networks. The proposed task-specific expert networks are trained and tested on five large-scale datasets, namely RESIDE [19], Haze4k [23], CSD [7], SRSS [6] and Snow100K [24]. For fair comparison, we follow the latest dehazing and desnowing

TABLE I: Quantitative comparisons of our framework with the state-of-the-art single image dehazing methods on Haze4k and SOTS outdoor dataset (PSNR(dB)/SSIM). The best results are **bold**, second best results are underlined.

Method	Haze4k [7]		SOTS Outdoor		#Param	#GMacs
	PSNR↑	SSIM↑	PSNR↑	SSIM↑		
(TPAMI'10)DCP [13]	14.01	0.76	15.09	0.76	-	-
(CVPR'16)NLD [2]	15.27	0.67	17.27	0.75	-	-
(TIP'16)DehazeNet [5]	19.12	0.84	22.46	0.85	0.01M	0.52G
(ICCV'17)GDN [22]	23.29	0.93	30.86	0.98	0.96M	21.49G
(CVPR'20)MSBDN [10]	22.99	0.85	23.36	0.87	31.35M	41.58G
(CVPR'20)DA [30]	24.03	0.90	27.76	0.938	1.64M	33.59G
(AAAI'20)FFA-Net [27]	26.97	0.95	<u>33.57</u>	<u>0.98</u>	4.6M	150.94G
(CVPR'21 Oral)PSD-FFA [9]	16.56	0.73	<u>15.29</u>	<u>0.72</u>	4.6M	150.94G
(ACMMM'21)DMT-Net [23]	<u>28.53</u>	0.96	-	-	54.9 M	80.71G
Dehazing Expert-Net	29.12	<b>0.97</b>	33.59	<b>0.99</b>	1.14M	12.00G
Dehazing Expert-Net-Tiny	28.18	0.96	32.09	0.98	288K	3.06G
DAN-Net	<b>29.24</b>	<b>0.97</b>	<b>33.69</b>	<b>0.99</b>	2.73M	31.36G
DAN-Net-Tiny	28.56	0.96	32.24	0.98	1.02M	13.47G

method [7], [23] for the benchmark setting. In addition, we randomly choose 1000 paired data from hazy or snowy datasets respectively to train the proposed DAN-Net.

### B. Training Settings

We augment the training dataset with randomly rotated by 90, 180, 270 degrees and horizontal flip. The training image patches with the size  $256 \times 256$  are extracted as input images of our networks. The Adam optimizer is used with initial learning rate of  $2 \times 10^{-4}$ , and we employ the CyclicLR to adjust the learning rate, where on the triangular mode, the value of gamma is 1.0, base momentum is 0.9, max learning rate is  $3 \times 10^{-4}$  and base learning rate is the same as initial learning rate. We adopt the PyTorch to implement all the networks with 4 Tesla V100 GPU with total batchsize of 40. The  $\lambda_{st}$  as trade-off weight is set as 0.2 in all experiments.

### C. Comparison with State-of-the-art Methods

**Comparisons of Dehazing Results:** In Table I, we summarize the performance of our Dehazing expert network (Tiny), DAN-Net (Tiny) and state-of-the-art dehazing methods [2], [5], [9], [10], [13], [22], [23], [27], [30] on Haze4k [23] and SOTS [19]. By analyzing Table I, the proposed DAN-Net achieves the best performance with 29.24dB PSNR and 0.97 SSIM on the test dataset of Haze4k. Furthermore, the tiny version of DAN-Net also achieves 28.62 dB PSNR and 0.96 SSIM on the test dataset of Haze4k with impressive fewer computation and parameters. The quantitative comparisons verify that our proposed task-specific dehazing network (Dehazing Expert-Net and Dehazing Expert-Net-Tiny) and DAN-Net (DAN-Net and DAN-Net-Tiny) can guarantee superior performance with lower computational complexity for the dehazing task compared with other prevalent algorithms.

**Comparisons of Desnowing Results:** To reveal the desnowing performance of the proposed expert network and DAN-Net, the quantitative comparisons with state-of-the-art desnowing [6], [7], [11], [20], [24] and all-in-one network [20] methods are also conducted on the widely used benchmarks (i.e. CSD [7], SRRS [6] and Snow100K [24]), as depicted

in Table II. From Table II, the proposed expert network (Desnowing Expert-Net and Desnowing Expert Net-Tiny) and DAN-Net (DAN-Net and DAN-Net-Tiny) show the better desnowing performance for both PSNR and SSIM values.

**Comparison of Visual Effects:** We also conduct the visual comparisons with state-of-the-art dehazing and desnowing methods on synthetic and real-world hazy images. In order to verify the desnowing and dehazing performance of the proposed DAN-Net, the synthetic snowy image with haze interference are used for comparisons and the processed results by different algorithms are revealed in Fig. 3. In comparisons, four specialized dehazing methods (i.e. MSBDN [10], FFA [27], DA [30] and PSD [9]) only remove the haze and are unable to handle the snow particles with different size. The desnowing methods, JSTASR [6] and HDCW [7], can effectively alleviate the snow degradations, whereas the residual snowflakes still exist in these snow removal results due to the insufficient desnowing ability. Furthermore, the hazes cannot be removed thoroughly because JSTASR [6] and HDCW [7] are incapable of dealing with multiple degradations. Compared with these above methods, our proposed DAN-Net can simultaneously achieve image dehazing and desnowing and the restoration results are more closer to the ground truths. For the real-world winter degraded images, the visual comparisons are also performed in Fig. 4. As observed in Fig. 4, the dehazing approaches cannot address the snow degradations and two specialized desnowing methods cannot obtain the satisfactory results for real-world snowy images because the residual snow streaks still remain in the restoration results. In addition, the details influenced by the haze cannot also be recovered well, such as in the second row of Fig. 4.

For single image dehazing task, the visual comparisons are conducted on synthetic and real-world hazy images to verify the effectiveness of the proposed DAN-Net. As can be seen in Fig. 5 and 6, previous state-of-the-art dehazing algorithms cannot effectively remove the uneven haze effects and the obvious hazes remain in the restoration results. By contrast, the proposed DAN-Net outperforms other specialized dehazing methods in the aspect of visual effects for synthetic and real-

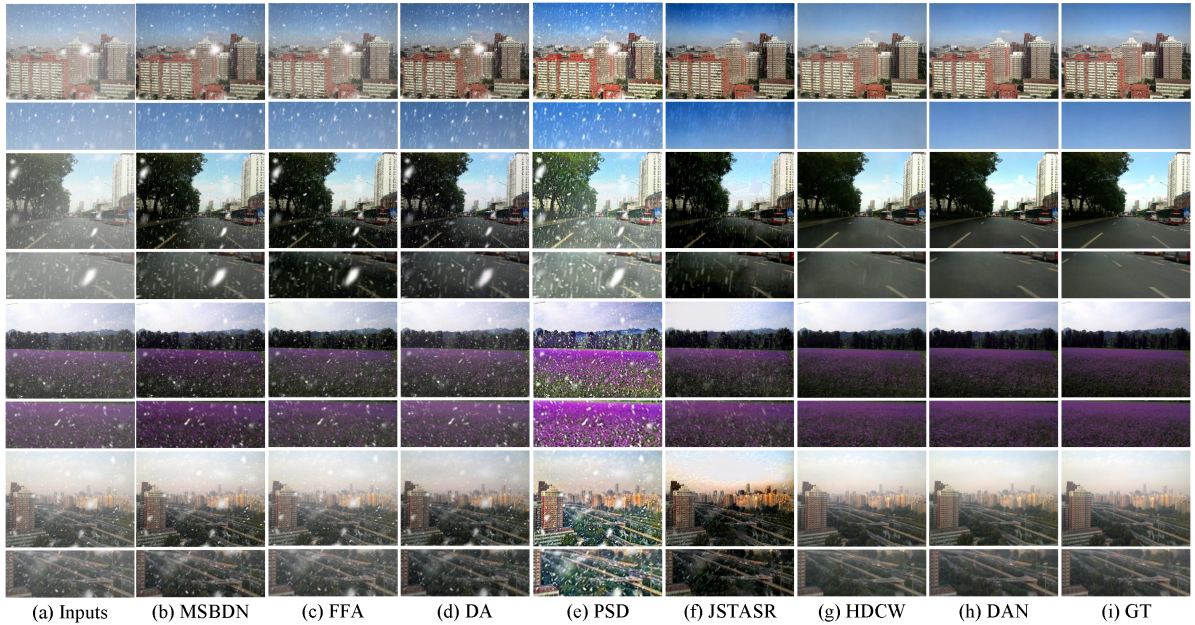


Fig. 3: Visual comparisons of desnowing results on synthetic snowy images from CSD dataset [7]. (a) and (i) are the input snowy images with haze interference and the ground truths. (b)-(g) are processed results respectively produced by MSBDN [10], FFA [27], DA [30], PSD [9], JSTASR [6] and HDCW [7]. (h) are our results yielded by DAN-Net.

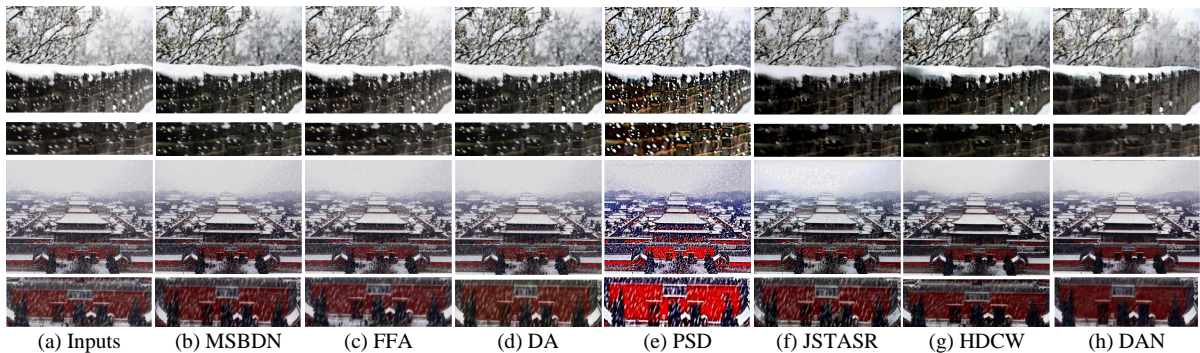


Fig. 4: Visual comparisons of desnowing results on real-world snowy images. (a) are the input snowy images. (b)-(g) are processed results respectively produced by MSBDN [10], FFA [27], DA [30], PSD [9], JSTASR [6] and HDCW [7]. (h) are our results yielded by DAN-Net.



Fig. 5: Visual comparisons of dehazing results on synthetic hazy images from Haze4K [23]. (a) and (h) are the input hazy image and the corresponding ground truths. (b)-(g) are the dehazed results respectively produced by MSBDN [10], FFA [27], AOD [18], GDN [22] and PSD [9]. (h) are the dehazed results by the proposed DAN-Net.

TABLE II: Quantitative comparisons of our expert networks and DAN-Net(Tiny) with the state-of-the-art desnowing methods on CSD, SRRS and Snow 100K desnowing dataset (PSNR(dB)/SSIM). The best results are shown in **bold**, and second best results are underlined.

Method	CSD(2000)		SRRS (2000)		Snow 100K (2000)		#Param	#GMacs
	PSNR	SSIM	PSNR	SSIM	PSNR	SSIM		
(TIP'18)Desnow-Net [24]	20.13	0.81	20.38	0.84	30.50	0.94	15.6M	-
(ICCV'17)CycleGAN [11]	20.98	0.80	20.21	0.74	26.81	0.89	7.84M	42.38G
(CVPR'20)All-in-One [20]	26.31	0.87	24.98	0.88	26.07	0.88	44 M	12.26G
(ECCV'20)JSTASR [6]	27.96	0.88	25.82	0.89	23.12	0.86	65M	-
(ICCV'21)HDCW-Net [7]	<u>29.06</u>	<u>0.91</u>	<u>27.78</u>	<u>0.92</u>	<u>31.54</u>	<u>0.95</u>	6.99M	9.78G
Desnowing Expert-Net	30.56	<b>0.95</b>	29.07	<b>0.95</b>	32.14	<b>0.96</b>	1.1M	12.00G
Desnowing Expert-Net-Tiny	29.06	0.92	28.20	0.94	31.67	0.95	288K	3.06G
DAN-Net	<b>30.82</b>	<b>0.95</b>	<b>29.34</b>	<b>0.95</b>	<b>32.48</b>	<b>0.96</b>	2.73M	31.36G
DAN-Net-Tiny	29.12	0.92	28.32	0.94	31.93	0.95	1.02M	13.47G

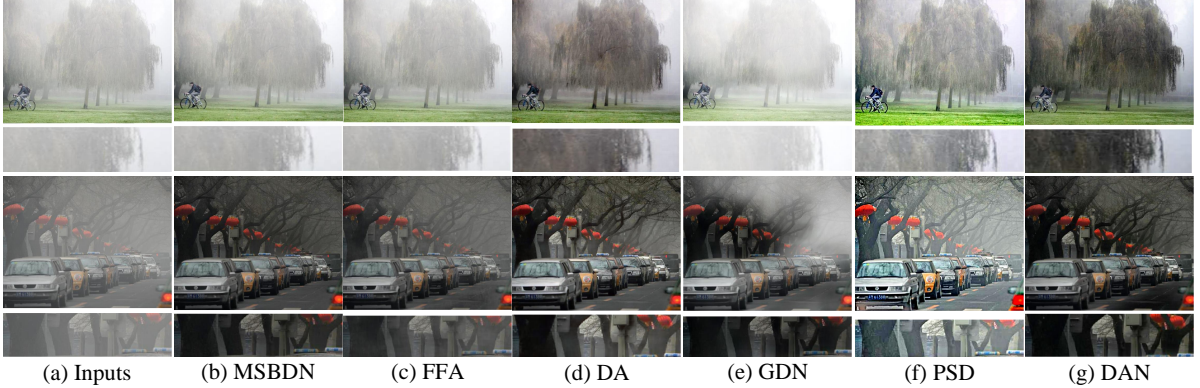


Fig. 6: Visual comparisons of dehazing results on real-world hazy images. (a) are the input hazy image. (b)-(f) are the dehazed results respectively produced by MSBDN [10], FFA [27], DA [30], GDN [22] and PSD [9]. (g) are the dehazed results by the proposed DAN-Net.

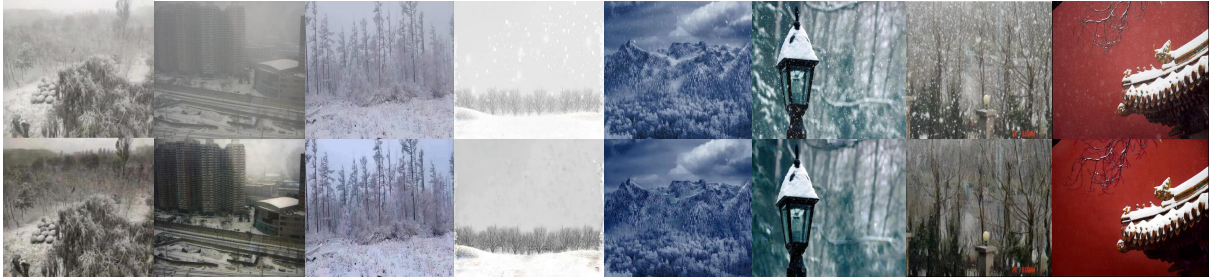


Fig. 7: Real-world winter images (top) and corresponding restoration results (bottom) using the proposed DAN-Net.

world scenarios.

Furthermore, more degraded images acquired by the real-world winter scene and the corresponding restoration results are revealed in Fig. 7 to demonstrate the robustness of the proposed DAN-Net. From the bottom row of Fig. 7, our proposed network can provide haze-free and snow-free restoration images with more details.

**Comparison of Computational Complexity:** For real-time deployment of models, the computational complexity is an important factor to consider. To check the computational complexity, we summarize the number of GMacs and parameters of previous state-of-the-art desnowing and dehazing networks in Table I and II. It is obviously found that the tiny desnowing expert network achieves best parameter-performance trade-off compared with the latest state-of-the-art desnowing method HDCW-Net (ICCV'21) and the number of GMacs is only 3.06G for the input size of  $256 \times 256$ .

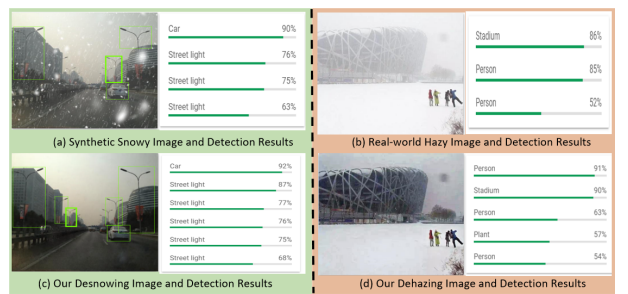


Fig. 8: Synthetic and real-world winter degenerated images (top) and corresponding restoration results (bottom) of the proposed DAN-Net with labels and confidences by Google Vision API.

**Quantifiable Performance for High-level Vision Tasks:** To verify the effectiveness of the proposed algorithm for high-level vision tasks, we adopt Google Vision API<sup>1</sup> to reveal

<sup>1</sup>Google Vision API : <https://cloud.google.com/vision/>

the subjective but quantifiable examples, as seen in Fig. 8. In Fig. 8, the degradations can impede the performance of high-level vision tasks and our restoration results have higher visibility and confidences for multiple labels, which deduces that our proposed DAN-Net contributes to high-level vision tasks.

#### D. Ablation Study

To demonstrate the contribution of the proposed modules, the ablation study is conducted. We make use of the widely used desnowing and dehazing datasets (i.e. CSD [7] and Haze4k [23]) for training and evaluation. Next, the effectiveness of three components and the loss function are verified.

**Effectiveness of MSTB:** To prove the superior performance of spectral transform for network training, we replace the global branch with plain Conv-ELU-Conv branch in the proposed network. Specifically, in Table III, we respectively adopt the vanilla convolution with kernel size  $3 \times 3$  (**VC**), the Local-branch (**LB**), the Global-branch (**GB**), the MSTB without spectral transform operation (**MSTBwoST**) and the complete MSTB (**Ours**) to evaluate the dehazing and desnowing performance of the proposed network with different MSTB configurations. From Table III, the designed spectral transform for the degradation feature extraction technique can achieve better recovered results compared with other configurations.

TABLE III: Comparisons of the performance of the proposed expert network with different MSTB configurations.

Metric	VC	LB	GB	MSTBwoST	Ours
Desnowing PSNR/SSIM	27.13/0.91	27.43/0.92	27.92/0.91	28.21/0.92	<b>30.56 / 0.95</b>
Dehazing PSNR/SSIM	26.53/0.93	26.69/0.93	26.73/0.93	27.05/0.94	<b>29.12/0.97</b>

**Effectiveness of DPAM:** To verify the effectiveness of the proposed DPAM, we construct several settings for comparison, that is, (i) The proposed expert network without DPAM (**wo DPAM**); (ii) Remove the Channel Attention Part (**CA**) of the attention module in the proposed DPAM. (iii) Remove the Spatial Attention Part (**CA**) of the attention module in the proposed DPAM. By analyzing Table IV, the quantitative results indicate that the performance of the expert networks with the proposed complete DPAM can be improved greatly compared with other settings.

TABLE IV: Comparisons of the performance of the proposed expert networks with different DPAM configurations.

Metrics	wo DPAM	CA	PA	Ours
Desnowing PSNR/SSIM	28.76/0.93	29.31/0.94	29.67/0.94	<b>30.56/0.95</b>
Dehazing PSNR/SSIM	28.15/0.94	28.57/0.96	28.68/0.96	<b>29.12/0.97</b>

**Effectiveness of CLAGM:** In the proposed CLAGM, the external information from the down-sampled original image is adopted to regulate the input features for better performance. The ablation experiments are performed to demonstrate the effectiveness of the regulation mechanism. As observed in Fig. 9, we provide six configurations of CLAGM. The performance of different configurations is depicted in Tab. V. In comparison, the proposed expert networks with the complete CLAGM exhibit highest PSNR and SSIM values, which indicates the effectiveness of the proposed CLAGM.

TABLE V: Comparisons of the performance of the proposed expert networks with different CLAGM configurations.

Configurations	A	B	C	D	E	Ours
Desnowing PSNR/SSIM	29.29 / 0.93	29.48 / 0.93	29.97 / 0.94	30.29 / 0.94	30.32 / 0.95	<b>30.56 / 0.95</b>
Dehazing PSNR/SSIM	27.73 / 0.94	28.11 / 0.95	28.30 / 0.95	28.49 / 0.96	28.92 / 0.97	<b>29.12 / 0.97</b>

TABLE VI: Effectiveness of the proposed loss functions.

Metrics	Baseline	$\mathcal{L}_{char}$	$\mathcal{L}_{char} + \mathcal{L}_{per}$	Ours
Desnowing PSNR/SSIM	29.26 / 0.92	29.44 / 0.92	30.13 / 0.93	30.56 / 0.95
Dehazing PSNR/SSIM	28.42 / 0.94	28.56 / 0.95	28.73 / 0.96	29.12 / 0.97

**Effectiveness of loss function:** For the loss function, we also perform the ablation experiments for demonstrate the effectiveness of the used loss function in the proposed network, as shown in Table VI. The ‘**Baseline**’ means using the classic  $L_1$  loss on the final recovered result. In addition, we also respectively consider the perceptual loss function  $\mathcal{L}_{per}$  and  $\mathcal{L}_{char} + \mathcal{L}_{per}$  loss function to train our network. From Table VI, our designed overall loss function reveals the best dehazing and desnowing performance.

## VII. CONCLUSIONS

In this paper, a lightweight degradation-adaptive neural network called DAN-Net to jointly remove haze and snow degradations under real-world nasty winter scenes is proposed. First, to handle the complicated snowy or hazy scenario, the task-specific expert networks comprising of three designed compact components are developed to achieve better trade-off between restoration performance of dehazing and desnowing and parameters. More importantly, a novel adaptive gated neural based on the MoE strategy is presented, which can adaptively handle the complex winter degradation by the haze and snow. Experimental results demonstrate that the proposed approach outperforms state-of-the-art dehazing and desnowing algorithms and is also capable of contributing to high-level vision tasks.

## VIII. ACKNOWLEDGEMENTS

This work was supported in part by Natural Science Foundation of Chongqing, China (cstc2020jcyjmsxmX0324), the project of science and technology research program of Chongqing Education Commission of China (Grant No. KJQN202200206), the Natural Science Foundation of Fujian Province of China (2021J01867), Education Department of Fujian Province (JAT190301), Foundation of Jimei University (ZP2020034).

## REFERENCES

- [1] R. Aljundi, P. Chakravarty, and T. Tuytelaars, “Expert gate: Lifelong learning with a network of experts,” in *Proceedings of the IEEE Conference on Computer Vision and Pattern Recognition*, 2017, pp. 3366–3375.
- [2] D. Berman, S. Avidan *et al.*, “Non-local image dehazing,” in *Proceedings of the IEEE conference on computer vision and pattern recognition*, 2016, pp. 1674–1682.
- [3] D. Berman, T. Treibitz, and S. Avidan, “Single image dehazing using haze-lines,” *IEEE transactions on pattern analysis and machine intelligence*, vol. 42, no. 3, pp. 720–734, 2018.
- [4] T. M. Bui and W. Kim, “Single image dehazing using color ellipsoid prior,” *IEEE Transactions on Image Processing*, vol. 27, no. 2, pp. 999–1009, 2017.

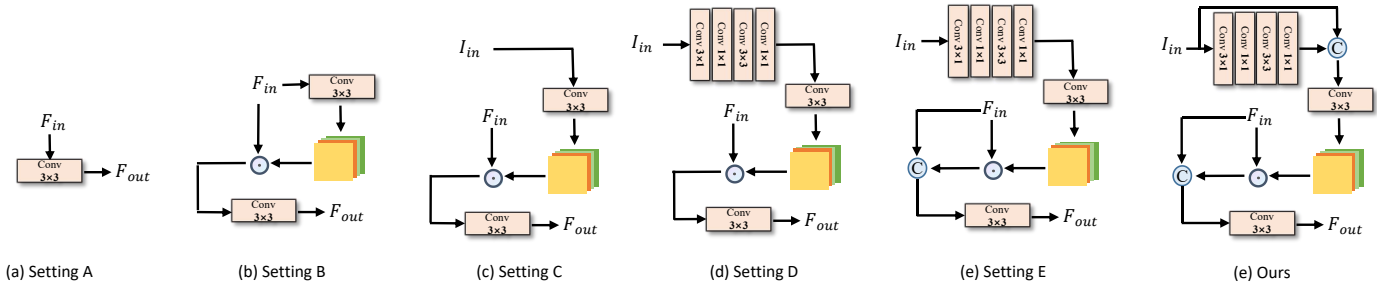


Fig. 9: Different configurations of CLAGM for ablation study.

- [5] B. Cai, X. Xu, K. Jia, C. Qing, and D. Tao, "Dehazenet: An end-to-end system for single image haze removal," *IEEE Transactions on Image Processing*, vol. 25, no. 11, pp. 5187–5198, 2016.
- [6] W. T. Chen, H.-Y. Fang, J.-J. Ding, C.-C. Tsai, and S.-Y. Kuo, "Jstar: Joint size and transparency-aware snow removal algorithm based on modified partial convolution and veiling effect removal," in *European Conference on Computer Vision*. Springer, 2020, pp. 754–770.
- [7] W.-T. Chen, H.-Y. Fang, C.-L. Hsieh, C.-C. Tsai, I. Chen, J.-J. Ding, S.-Y. Kuo *et al.*, "All snow removed: Single image desnowing algorithm using hierarchical dual-tree complex wavelet representation and contradict channel loss," in *Proceedings of the IEEE/CVF International Conference on Computer Vision*, 2021, pp. 4196–4205.
- [8] W.-T. Chen, Z.-K. Huang, C.-C. Tsai, H.-H. Yang, J.-J. Ding, and S.-Y. Kuo, "Learning multiple adverse weather removal via two-stage knowledge learning and multi-contrastive regularization: Toward a unified model," in *Proceedings of the IEEE/CVF Conference on Computer Vision and Pattern Recognition (CVPR)*, June 2022, pp. 17653–17662.
- [9] Z. Chen, Y. Wang, Y. Yang, and D. Liu, "Psd: Principled synthetic-to-real dehazing guided by physical priors," in *Proceedings of the IEEE/CVF Conference on Computer Vision and Pattern Recognition*, 2021, pp. 7180–7189.
- [10] H. Dong, J. Pan, L. Xiang, Z. Hu, X. Zhang, F. Wang, and M.-H. Yang, "Multi-scale boosted dehazing network with dense feature fusion," in *Proceedings of the IEEE/CVF Conference on Computer Vision and Pattern Recognition*, 2020, pp. 2157–2167.
- [11] D. Engin, A. Genç, and H. Kemal Ekenel, "Cycle-dehaze: Enhanced cyclegan for single image dehazing," in *Proceedings of the IEEE Conference on Computer Vision and Pattern Recognition Workshops*, 2018, pp. 825–833.
- [12] R. Fattal, "Dehazing using color-lines," *ACM transactions on graphics (TOG)*, vol. 34, no. 1, pp. 1–14, 2014.
- [13] K. He, J. Sun, and X. Tang, "Single image haze removal using dark channel prior," *IEEE transactions on pattern analysis and machine intelligence*, vol. 33, no. 12, pp. 2341–2353, 2011.
- [14] R. A. Jacobs, M. I. Jordan, S. J. Nowlan, and G. E. Hinton, "Adaptive mixtures of local experts," *Neural computation*, vol. 3, no. 1, pp. 79–87, 1991.
- [15] M. Ju, C. Ding, C. A. Guo, W. Ren, and D. Tao, "Idrlp: Image dehazing using region line prior," *IEEE Transactions on Image Processing*, vol. 30, pp. 9043–9057, 2021.
- [16] M. Ju, C. Ding, Y. J. Guo, and D. Zhang, "Idgcp: Image dehazing based on gamma correction prior," *IEEE Transactions on Image Processing*, vol. 29, pp. 3104–3118, 2019.
- [17] R. Kumar, A. K. Bhandari, and M. Kumar, "Haze elimination model based color saturation adjustment with contrast correction," *IEEE Transactions on Instrumentation and Measurement*, vol. 71, p. 5013610, 2022.
- [18] B. Li, X. Peng, Z. Wang, J. Xu, and D. Feng, "Aod-net: All-in-one dehazing network," in *Proceedings of the IEEE international conference on computer vision*, 2017, pp. 4770–4778.
- [19] B. Li, W. Ren, D. Fu, D. Tao, D. Feng, W. Zeng, and Z. Wang, "Benchmarking single-image dehazing and beyond," *IEEE Transactions on Image Processing*, vol. 28, no. 1, pp. 492–505, 2018.
- [20] R. Li, R. T. Tan, and L.-F. Cheong, "All in one bad weather removal using architectural search," in *Proceedings of the IEEE/CVF Conference on Computer Vision and Pattern Recognition*, 2020, pp. 3175–3185.
- [21] C. Lin, X. Rong, and X. a. Yu, "Msaff-net: Multiscale attention feature fusion networks for single image dehazing and beyond," *IEEE Transactions on Multimedia*, 2022.
- [22] X. Liu, Y. Ma, Z. Shi, and J. Chen, "Griddehazenet: Attention-based multi-scale network for image dehazing," in *Proceedings of the IEEE/CVF International Conference on Computer Vision*, 2019, pp. 7314–7323.
- [23] Y. Liu, L. Zhu, S. Pei, H. Fu, J. Qin, Q. Zhang, L. Wan, and W. Feng, "From synthetic to real: Image dehazing collaborating with unlabeled real data," in *Proceedings of the 29th ACM International Conference on Multimedia*, 2021, pp. 50–58.
- [24] Y.-F. Liu, D.-W. Jaw, S.-C. Huang, and J.-N. Hwang, "Desnownet: Context-aware deep network for snow removal," *IEEE Transactions on Image Processing*, vol. 27, no. 6, pp. 3064–3073, 2018.
- [25] S. Pavlitskaya, C. Hubschneider, M. Weber, R. Moritz, F. Huger, P. Schlicht, and M. Zollner, "Using mixture of expert models to gain insights into semantic segmentation," in *Proceedings of the IEEE/CVF Conference on Computer Vision and Pattern Recognition Workshops*, 2020, pp. 342–343.
- [26] S. C. Pei, Y. T. Tsai, and C. Y. Lee, "Removing rain and snow in a single image using saturation and visibility features," in *IEEE International Conference on Multimedia and Expo Workshops*, 2014.
- [27] X. Qin, Z. Wang, Y. Bai, X. Xie, and H. Jia, "Ffa-net: Feature fusion attention network for single image dehazing," in *Proceedings of the AAAI Conference on Artificial Intelligence*, vol. 34, no. 07, 2020, pp. 11908–11915.
- [28] W. Ren, S. Liu, H. Zhang, J. Pan, X. Cao, and M.-H. Yang, "Single image dehazing via multi-scale convolutional neural networks," in *European conference on computer vision*. Springer, 2016, pp. 154–169.
- [29] L. M. Schiapparelli, P. Sharma, H.-Y. He, J. Li, S. H. Shah, D. B. McClatchy, Y. Ma, H.-H. Liu, J. L. Goldberg, J. R. Yates III *et al.*, "Proteomic screen reveals diverse protein transport between connected neurons in the visual system," *Cell Reports*, vol. 38, no. 4, p. 110287, 2022.
- [30] Y. Shao, L. Li, W. Ren, C. Gao, and N. Sang, "Domain adaptation for image dehazing," in *Proceedings of the IEEE/CVF conference on computer vision and pattern recognition*, 2020, pp. 2808–2817.
- [31] Y. Wang, S. Liu, C. Chen, and B. Zeng, "A hierarchical approach for rain or snow removing in a single color image," *IEEE Transactions on Image Processing*, pp. 3936–3950, 2017.
- [32] J. Xu, W. Zhao, P. Liu, and X. Tang, "An improved guidance image based method to remove rain and snow in a single image," *Computer and Information Science*, vol. 5, no. 3, 2012.
- [33] J. Xu, W. Zhao, P. Liu, and X. Tang, "Removing rain and snow in a single image using guided filter," in *2012 IEEE International Conference on Computer Science and Automation Engineering (CSAE)*, vol. 2. IEEE, 2012, pp. 304–307.
- [34] X. Zheng, Y. Liao, W. Guo, X. Fu, and X. Ding, "Single-image-based rain and snow removal using multi-guided filter," in *International Conference on Neural Information Processing*. Springer, 2013, pp. 258–265.
- [35] S. Zhou, X. Liu, J. Duan, and F. Herz, "A novel model-based defogging method for particle images with different fog distributions," *IEEE Transactions on Instrumentation and Measurement*, vol. 71, p. 5008719, 2022.
- [36] Q. Zhu, J. Mai, and L. Shao, "A fast single image haze removal algorithm using color attenuation prior," *IEEE transactions on image processing*, vol. 24, no. 11, pp. 3522–3533, 2015.
- [37] Z. Zhu, H. Wei, G. Hu, Y. Li, G. Qi, and N. Mazur, "A novel fast single image dehazing algorithm based on artificial multiexposure image fusion," *IEEE Transactions on Instrumentation and Measurement*, vol. 70, p. 5001523, 2021.